Cipulli *et al. J Anesth Analg Crit Care* (2026) 6:20
https://doi.org/10.1186/s44158-025-00320-4

Journal of Anesthesia, Analgesia and Critical Care

REVIEW

Open Access

Dead space in critical care: a practical approach with clinical scenarios

Francesco Cipulli[1], Andrea Sanna[1], Roberta Garberi[2], Sergio Lassola[1], Mario Forcione[2], Giacomo Bellani[1,4], Giuseppe Foti[2,3] and Emanuele Rezoagli[2,3*]

Abstract

Carbon dioxide (CO_2) is a byproduct of cellular metabolism, with the human body storing approximately 120 liters in various chemical forms across different compartments. Through gas exchange and tidal ventilation, arterial CO_2 and blood pH are tightly regulated within the narrow ranges required for cellular function. Not all tidal ventilation, however, contributes to CO_2 elimination: the portion of each breath that does not participate in gas exchange is defined as dead space. First described in 1891 by Christian Bohr in his seminal work *"Über die Lungenatmung"*, the concept gained practical applicability in 1938 when Enghoff proposed replacing the unmeasurable alveolar partial pressure CO_2 ($PACO_2$) with the arterial partial pressure of CO_2 ($PaCO_2$) in the calculation. Since then, dead space has become a cornerstone parameter for quantifying the severity of respiratory failure. Recent advances in lung imaging have expanded the possibilities for assessing dead space distribution by integrating anatomical and functional information. Techniques such as contrast-enhanced computed tomography (CT), dual-energy CT (DECT), magnetic resonance imaging (MRI), and, increasingly, electrical impedance tomography (EIT) now offer novel opportunities to visualize and quantify regional ventilation–perfusion (V/Q) mismatch. In this narrative review, we outline the mathematical foundations of dead space computation and examine the role of each variable in the calculation. We then explore derived indices such as the ventilatory ratio and standardized minute ventilation. Finally, we discuss recent technological innovations, including EIT, MRI, and CT, and present clinical cases to illustrate the practical application of dead space assessment in daily clinical practice.

Keywords Respiratory failure, ARDS, Dead space, Pulmonary shunt, Electrical impedance tomography, Volumetric capnography

Background

Respiratory failure is defined as the inability to achieve adequate oxygenation and/or carbon dioxide elimination through gas exchange [1]. It can be broadly categorized into two types: hypoxemic respiratory failure, where oxygenation is predominantly impaired, and hypercapnic (ventilatory) failure, where carbon dioxide clearance is the primary issue [2]. Two key parameters, pulmonary shunt and dead space, are integral in assessing the severity of respiratory failure [3]. Pulmonary shunt, resulting from the perfusion of non-ventilated alveoli, plays a major role in the hypoxemic component of respiratory failure, whereas dead space—arising from the ventilation of non-perfused alveoli—is primarily associated with its hypercapnic component [4, 5]. Both concepts are fundamental to understand and treat acute respiratory failure effectively [6, 7]. Given the critical clinical relevance of

*Correspondence:
Emanuele Rezoagli
emanuele.rezoagli@unimib.it
[1] Anesthesia and Intensive Care 1, Santa Chiara Hospital, APSS, Largo Medaglie d'Oro 9, Trento 38112, Italy
[2] School of Medicine and Surgery, University of Milano-Bicocca, Via Cadore 48, Monza 20900, Italy
[3] Department of Emergency and Intensive Care, Fondazione IRCCS San Gerardo Dei Tintori, Via Pergolesi 33, Monza 20900, Italy
[4] Centre for Medical Sciences-CISMed, University of Trento, Via S. Maria Maddalena 1, Trento 38122, Italy

dead space in clinical practice [8], this narrative review traces its evolution from its initial physiological description in the nineteenth century to its modern-day applications and physiological surrogates. Further, we present clinical cases to illustrate the practical use of the dead space concept in daily medical practice, emphasizing its role in optimizing patient management.

Section 1—physiological basis of dead space

Concepts of CO_2 production and elimination: the VCO_2

CO_2 is a byproduct of cellular metabolism. The human body stores approximately 120 L of CO_2 in various chemical forms across different compartments. The majority (up to 89%) is stored as bicarbonates and carbonates in the bone, commonly referred to as the "slow compartment." The remaining CO_2 (11%) is distributed between the interstitium (8.5%) and blood (2.5%), collectively known as the "fast compartment" [9].

In the bloodstream, most CO_2 produced by peripheral tissues is transported as bicarbonate (HCO_3^-) in plasma, formed through the hydration of CO_2 according to the reaction $CO_2 + H_2O \rightleftharpoons H_2CO_3 \rightleftharpoons H^+ + HCO_3^-$, which depends on the CO_2 solubility coefficient and blood pH as described in the following equation [10, 11]:

$$HCO_3^- = 0.0306 * PCO_2 * 10^{(ph-pk)}$$

A smaller fraction is transported physically dissolved in plasma (≈5–10%) or bound to hemoglobin as carbamino compounds (≈10–20%). The $PaCO_2$ reflects the balance between tissue CO_2 production and the respiratory elimination. When equilibrium is achieved (constant $PaCO_2$), the rate of CO_2 production matches the rate of CO_2 exhalation. The corresponding volume of CO_2 produced and exhaled per minute is referred to as VCO_2 [10]. In a healthy, resting adult, VCO_2 typically ranges between 3 and 4 mL/kg/min (for a 70-kg individual, approximately 210–280 mL/min). However, VCO_2 can increase significantly during hypermetabolic states such as exercise, fever, or sepsis [10, 12].

Through gas exchange and tidal ventilation, $PaCO_2$ and blood pH are maintained within normal ranges (35–45 mmHg and 7.35–7.45, respectively). However, not all tidal ventilation contributes to alveolar ventilation: the portion of each breath that does not participate in gas exchange is termed dead space [13].

Dead space computation: the Bohr equation and the Enghoff modification

Dead space was first described in 1891 by Bohr in his seminal work *"Über die Lungenatmung"* [14]. The Danish physiologist divided the tidal volume (VT) of an exhaled breath into two components: alveolar ventilation (VA), which participates in gas exchange, and dead space (VD), which does not.

This relationship is mathematically expressed as:

$V_T = V_A + V_D$

To quantify dead space, Bohr applied the principle of mass balance using CO_2. The underlying assumption is that dead space does not contribute CO_2 to the exhaled breath, while both tidal VT and VA do, based on their respective CO_2 fractions (FCO_2).

This relationship can be summarized as:

$V_T * F_ECO_2 = V_A * F_ACO_2 + V_D * F_DCO_2$

Since the CO_2 contribution from dead space (V_D * F_DCO_2) is effectively zero and V_A equals the difference between V_T and V_D, the equation simplifies to

$V_T * F_ECO_2 = (V_T - V_D) * F_ACO_2$

Expanding and rearranging terms yields:

$V_T * F_ECO_2 = V_T * F_ACO_2 - V_D * F_ACO_2$

$V_T * F_ECO_2 - V_T * F_ACO_2 = -V_D * F_ACO_2$

$V_T * F_ACO_2 - V_T * F_ECO_2 = V_D * F_ACO_2$

$V_T * (F_ACO_2 - F_ECO_2) = V_D * F_ACO_2$

The FCO_2 can be expressed in terms of the partial pressure of CO_2 (PCO_2), based on the relationship:

$PCO_2 = (P_{atm} - P_{vap}) * FCO_2$ where P_{atm} is atmospheric pressure (760 mmHg), and P_{vap} is water vapor pressure (47 mmHg). Substituting into the equation and rearranging, we derive:

$$\frac{Vd}{Vt} = \frac{(P_ACO_2 - P_ECO_2)}{P_ACO_2}$$

Here, V_D/V_T represents the dead space fraction, which is a key metric for assessing the efficiency of ventilation [14, 15]. This equation forms the basis of dead space calculation and continues to be a fundamental concept in respiratory physiology and clinical practice [7, 9] (Fig. 1).

Variables explanation: alveolar and arterial PCO_2

$PACO_2$ represents the partial pressure of CO_2 in the alveoli, reflecting the balance between CO_2 production and its elimination through ventilation [16]. However, accurately measuring $PACO_2$ in practice is nearly impossible due to its dependence on dynamic and unpredictable factors, such as the regional coupling between alveolar ventilation and perfusion [17]. In 1938, to overcome this challenge, Enghoff proposed substituting the unmeasurable $PACO_2$ with the $PaCO_2$ [18]. This substitution assumed that, under normal physiological conditions, equilibrium is achieved between arterial and alveolar CO_2 at the end of the gas exchange process. By leveraging this relationship, Enghoff's modification made the calculation of dead space feasible and practical. With the advent of blood gas analysis in the 1920 s, this method

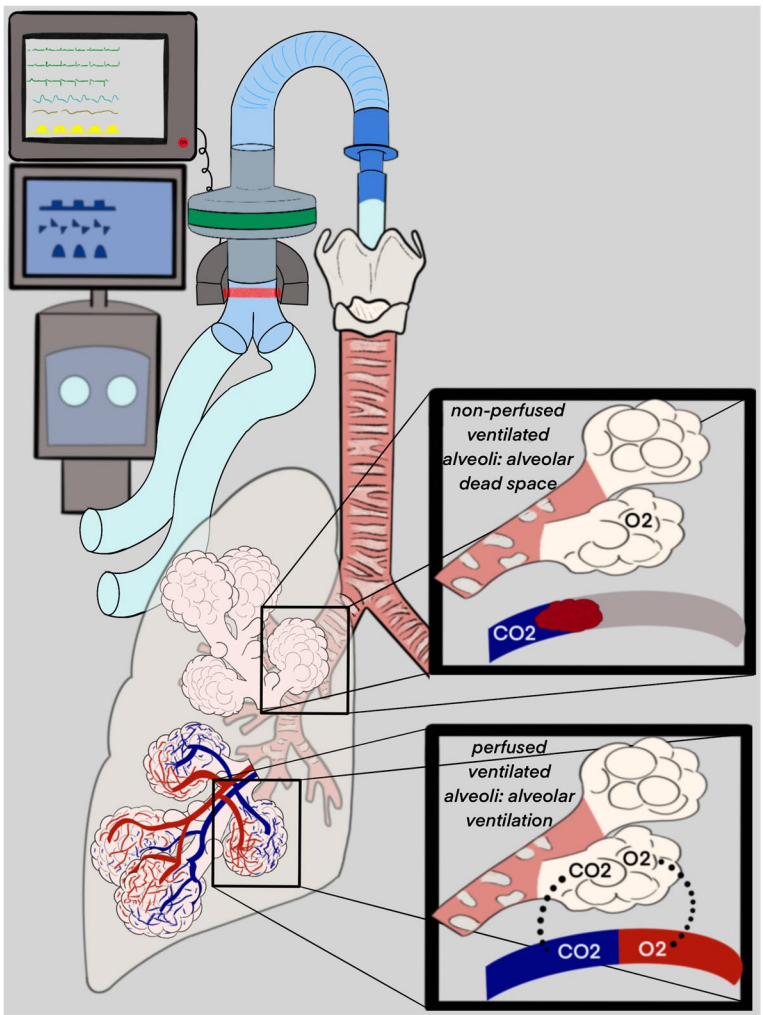

Fig. 1 Illustration of end-tidal CO_2 ($EtCO_2$) monitoring and dead space. The patient is mechanically ventilated via an endotracheal tube connected to a mount, a filter, an in-line airway CO_2 sensor, and a Y-piece. Infrared capnography measures CO_2 in the expiratory flow, providing continuous $EtCO_2$. The segment of circuit between the airway and the Y-piece constitutes *instrumental dead space*; the inspiratory and expiratory limbs beyond the Y-piece do not contribute to it. The conducting airways, from the tube tip to the terminal bronchioles, represent *anatomical dead space*, which does not participate to gas exchange. In the lower quadrant, ventilation and perfusion are matched: O_2 diffuses from alveoli into blood and CO_2 diffuses in opposite direction, leading to efficient gas exchange and $EtCO_2$ values close to $PaCO_2$. In the upper quadrant, unmatched ventilation and perfusion due to absent or reduced perfusion (e.g. pulmonary embolism) creates *alveolar dead space*, thereby increasing total dead space and typically lowering $EtCO_2$, widening the $PaCO_2$–$EtCO_2$ gradient at a given minute ventilation

facilitated the routine measurement of dead space in clinical practice [19, 20]. Despite its utility, Enghoff's modification is not without limitations. In certain pathological conditions, such as significant venous admixture caused by high pulmonary shunting, the arterial and alveolar CO_2 values may diverge substantially [21]. In these cases, $PaCO_2$ increases due to CO_2-rich blood bypassing the lungs, while $PACO_2$ decreases proportionally. This disparity can lead to an overestimation of dead space, as the computed value is based on an erroneously elevated $PaCO_2$. However, this effect is only pronounced when the pulmonary shunt exceeds 40%; for lower shunt values, the impact on dead space calculations remains negligible [22]. In this context, however, the measured dead space, rather than representing a pure overestimation, can be interpreted as a severity index or an indirect marker of gas exchange inefficiency, which becomes apparent primarily in clinical situations with a high pulmonary shunt fraction. Despite these limitations, Enghoff's modification continues to be the most widely used method in clinical practice today, providing a valuable tool for assessing ventilation efficiency in various settings.

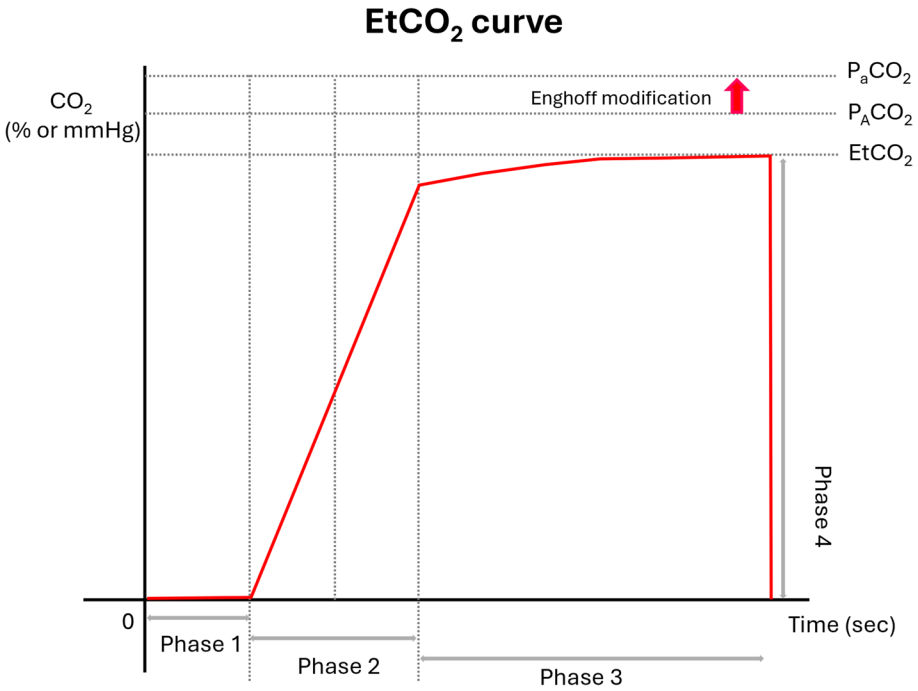

Fig. 2 $EtCO_2$ curve illustration. The expired CO_2 (expressed as concentration percentage or partial pressure on the *y*-axis) is plotted as a function of time (in seconds on the *x*-axis)

Variables explanation: end-tidal CO_2 and mixed expiratory CO_2

The CO_2 exhaled from the alveoli during expiration can be sampled at various locations along the respiratory circuit. One common sampling site is at the airway's distal end, just beyond the endotracheal tube [23]. The CO_2 measured at this location can then be recorded on a breath-by-breath basis. The curve depicting exhaled CO_2 variation (*Y*-axis) over time (*X*-axis) allows identification of the end-tidal CO_2 ($EtCO_2$), defined as the CO_2 concentration reached at the end of tidal expiration (Fig. 2).

The $EtCO_2$ curve is divided into four distinct phases:

- Phase 1: includes the inspiratory phase and the exhalation of the anatomical dead space, during which the PCO_2 equals that of the inhaled gas (typically atmospheric CO_2, which is near zero, resulting in a flat curve).
- Phase 2: marks the onset of CO_2 exhalation. Here, the CO_2 concentration rises as alveolar gas starts to mix with air from the anatomical dead space. It is important to note that Phase 2 does not correspond to the initiation of tidal volume exhalation (which begins earlier) but instead marks the start of detectable CO_2 exhalation.
- Phase 3: displays a semi-flat slope, representing the exhalation of alveolar gas. The slope reflects the time constants of the respiratory system [24, 25].
- Phase 4: denotes the end of tidal exhalation, during which the CO_2 concentration returns to zero as atmospheric air is sampled.

The $EtCO_2$ value reached during Phase 3 is then used to calculate the alveolar dead space, according to the following formula:

$$\frac{Vd}{Vt}Alv = \frac{(P_aCO_2 - EtCO_2)}{P_aCO_2}$$

For accurate dead space assessment, it is essential that the end-tidal CO_2 ($EtCO_2$) value remains stable during Phase 3 (plateau phase) of the capnographic waveform. This stability reflects a homogeneous alveolar gas composition at the end of expiration, ensuring that the measured $EtCO_2$ closely approximates true alveolar CO_2. Fluctuations or an absent plateau during this phase may indicate ventilation–perfusion mismatch, incomplete alveolar emptying, or technical artifacts, all of which can lead to inaccurate dead space calculation [22, 26] (Fig. 3).

Volumetric capnography provides a more detailed assessment, quantifying CO_2 elimination against the tidal volume. The volumetric capnography curve is also divided into four phases [27]:

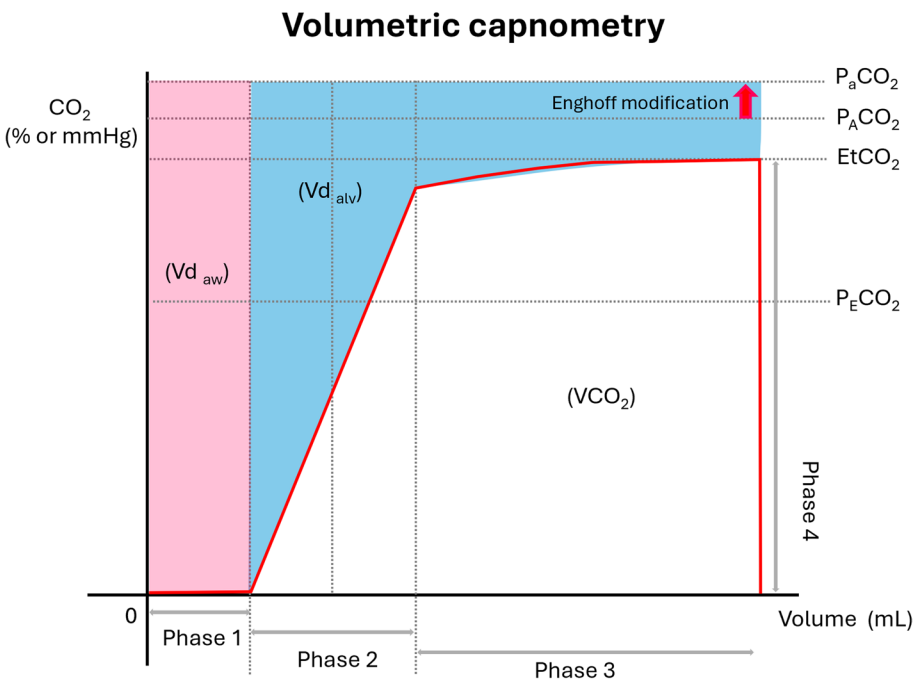

Fig. 3 Volumetric capnography illustration. The $EtCO_2$ (concentration percentage or partial pressure; *y*-axis) is expressed as a function of expiratory volume (mL; *x*-axis). Notably, the pink area represents the anatomical dead space, the blue area corresponds to the alveolar space, and the area below the red line indicates the volume of expired CO_2 in each breath

- Phase 1: represents the exhalation of the anatomical dead space, which does not contain CO_2.
- Phase 2: depicts a progressive rise in CO_2 as the transition from anatomical dead space to alveolar ventilation occurs.
- Phase 3: shows an almost plateau-like region where CO_2 concentration verges to be relatively constant.
- Phase 4: marks the return of CO_2 levels to zero at the end of exhalation.

This curve defines two areas:

The area under the CO_2 curve, representing the total CO_2 exhaled during the breath (VCO_2 per breath). The area above the CO_2 curve, indicating the gas volume exhaled with a CO_2 pressure or fraction lower than arterial CO_2 which corresponds to the physiological dead space (anatomical plus alveolar dead space) [27].

Another key parameter derived from volumetric capnography is the mixed expiratory CO_2 ($PECO_2$). $PECO_2$ is calculated as the ratio between the area under the capnography curve and the tidal volume or measured directly via a sensor at the ventilator's exhaust [28]. This value reflects the average (mixed) CO_2 concentration during tidal exhalation and is used to calculate the physiological dead space as follows:

$$\frac{Vd}{Vt}phy = \frac{(P_aCO_2 - P_ECO_2)}{P_aCO_2}$$

Lastly, the anatomical dead space can be determined by subtracting the alveolar dead space from the physiological dead space [29].

Volumetric capnography provides extensive information about CO_2 exhalation and dead space assessment. Compared $EtCO_2$, it enables the calculation of physiological dead space rather than just alveolar dead space. However, not all ventilators are equipped to perform volumetric capnography or measure $PECO_2$. In such cases, $EtCO_2$ remains a more accessible and widely available tool for dead space evaluation (Fig. 4).

Dead space surrogates: ventilatory ratio and standardized minute ventilation

The Ventilatory Ratio (VR) is a practical and straightforward tool used to estimate ventilatory efficiency, offering insights into dead-space dynamics without the need for measuring expiratory PCO_2 directly. This simplicity makes it a widely applicable surrogate for assessing effective ventilation [30, 31].

VR is calculated using the following formula:

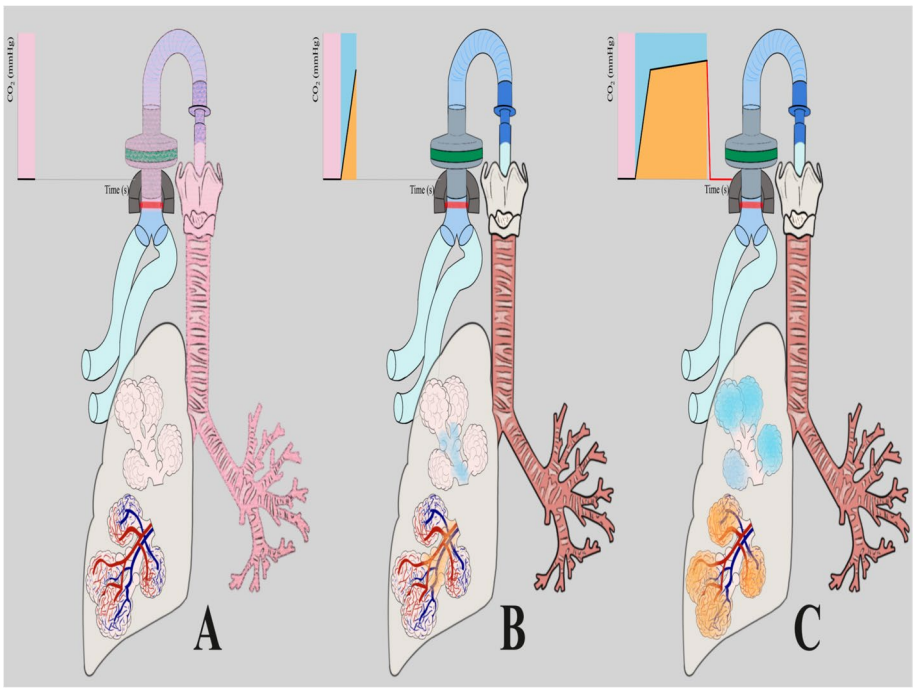

Fig. 4 Illustration of the capnography phases and its sites of origin. In the capnography: the CO_2 levels are in black and red for the expiration and inspiration, respectively; instrumental and anatomical dead spaces are in pink, alveolar dead space is in light blue, and volume of CO_2 (VCO_2) exhaled is in orange. **A** Phase 1: Dead-space washout. Exhalation of CO_2-free gas from the instrumental dead space and the patient's airway (anatomic dead space). **B** Phase 2: Transition to alveolar ventilation. Progressive rise in measured CO_2 as alveolar gas mixes with dead-space gas; the upstroke slope reflects the progressive emptying of all alveoli. **C** Phases 3–4: Alveolar plateau and inspiratory downstroke. CO_2 becomes relatively constant as the sample is predominantly alveolar gas; the end of the plateau is $EtCO_2$. Alveolar dead space steepens the plateau (increases Phase 3 slope) and lowers $EtCO_2$, widening the $PaCO_2$–$EtCO_2$ gradient. With inspiration, fresh gas flushes CO_2 back to approximately zero (a persistently elevated baseline suggests rebreathing)

$$VR = \frac{Ve * PaCO_2}{100 * BW * 37{,}5}$$

Here, Ve represents minute ventilation, BW refers to body weight in kilograms, and 37.5 mmHg is the assumed ideal $PaCO_2$. The numerator reflects the actual ventilation required to produce the measured $PaCO_2$, while the denominator represents the theoretical ventilation needed to maintain a normal $PaCO_2$ level of 37.5 mmHg [21, 30].

The interpretation of VR is intuitive:

VR > 1 suggests impaired ventilatory efficiency, often linked to increased dead space while VR ≤ 1 indicates normal or efficient ventilation. Importantly, a VR greater than 2 has been associated with higher mortality risk in patients with acute respiratory distress syndrome (ARDS), underscoring its clinical relevance [32]. To better understand why VR is considered a surrogate for dead space, we can explore its relationship with physiological parameters. By substituting the determinants of $PaCO_2$ and minute ventilation, the equation for VR reveals its direct dependence on CO_2 production (VCO_2) and the dead-space fraction (V_d/V_t) [33]:

$$VR = \frac{1}{k * BW} * \frac{863 * VCO_2}{1 - {}^{Vd}/_{Vt}}$$

This shows that VR increases with both higher CO_2 production and greater dead-space fraction. In essence, the more inefficient the ventilation, the higher the VR value. However, it is worth to remind that in conditions of significant pulmonary shunt, VR may overestimate dead space due to the overestimation of arterial CO_2 levels (see section on dead-space overestimation caused by high shunt fraction). Clinically, VR has proven to be a valuable prognostic marker in ARDS. Studies have shown that higher VR values independently correlate with increased hospital mortality, even after adjusting for markers of mechanical support and hypoxemia [34]. Furthermore, VR has been associated with the likelihood of successful respiratory weaning, further highlighting its utility in guiding clinical decisions [35].

Another useful metric for assessing ventilation efficiency is Standardized Minute Ventilation (SV), also known as corrected minute ventilation. SV is calculated as:

$$SV = Ve * \frac{PaCO_2}{40}$$

This measure reflects the ventilation required to normalize $PaCO_2$ to 40 mmHg. Like VR, higher SV values suggest increased dead-space fraction, providing another means of evaluating ventilatory inefficiency. Together, VR and SV offer accessible and clinically meaningful ways to assess ventilation and guide patient management, particularly in conditions like ARDS where dead space plays a pivotal role [33, 36].

Dead space surrogates: arterial to expiratory CO_2 gradient and ratio

During gas exchange, CO_2 from venous blood that passes through ventilated alveoli (non-shunted blood) diffuses into the alveolar space, contributing to alveolar CO_2. The remaining CO_2 in the blood—after gas exchange—becomes arterial capillary CO_2, which, when mixed with CO_2 from shunted blood, determines the arterial CO_2 concentration. In an ideal situation, with a shunt fraction of zero and steady-state conditions, the CO_2 content in venous capillary blood, alveolar gas, and arterial capillary blood would be identical. If arterial CO_2 remains constant, then the total amount of CO_2 produced metabolically (VCO_2 metabolic) must equal the amount eliminated by ventilation (VCO_2 respiratory). Although the total quantity of CO_2 remains the same, its measured concentration changes due to the presence of dead space. This can be conceptualized as a two-step dilution process of alveolar CO_2. The first dilution occurs in the alveolar dead space, which lowers alveolar CO_2 to produce the $EtCO_2$. The second dilution takes place in the anatomic dead space, further reducing CO_2 to yield the $PECO_2$.

In a hypothetical scenario without any dead space, $PaCO_2$, $EtCO_2$ and $PECO_2$ would all be equivalent [37]. In reality, the $PaCO_2$-$EtCO_2$ gradient is typically around 5 mmHg. However, in the presence of increased dead space (reduced $EtCO_2$) or shunting (elevated $PaCO_2$), this gradient can widen significantly [38]. Another valuable measure of gas exchange efficiency is the end-tidal to arterial CO_2 ratio ($EtCO_2/PaCO_2$). Ideally, this ratio is close to 1, indicating efficient ventilation and gas exchange. However, in conditions where dead space is increased or pulmonary shunting is significant, the ratio decreases. A value below 0.8 strongly indicates severe ventilatory impairment [39]. These relationships between CO_2 gradients and ratios provide crucial insights into gas exchange adequacy and the underlying physiological challenges, aiding in the assessment and management of respiratory conditions [40].

Dead space estimation: the automatic lung parameter (ALPE) system

The ALPE system was first described in 2002 by the Danish group led by Rees [41]. It is based on the non-invasive assessment of gas exchange in response to stepwise changes in FiO_2. The system comprises a ventilator, a gas analyzer, and a computer, and can be applied to both spontaneously breathing and mechanically ventilated patients. For mechanically ventilated patients, the ventilator is set according to standard clinical practice, while spontaneously breathing patients receive gas via a face mask. Continuous, breath-by-breath measurements include inspired and end-tidal gas fractions (FiO_2, FEO_2, $FECO_2$), respiratory rate, pulse and oxygen saturation (SpO_2). Ventilator parameters, including tidal volumes and respiratory frequency, are transmitted in real time to the computer alongside the gas analyzer data. FiO_2 is progressively increased in discrete steps, typically six increments. At each step, a new steady state is confirmed by a consistent difference between FiO_2 and FEO_2 before collecting the independent variables for input into the system. The collected data are analyzed using dedicated software implementing a complex mathematical model based on the Riley-Cournand gas exchange framework [42]. Upon completion, the system provides output variables such as shunt fraction, dead space, and the PaO_2/FiO_2 curve. In essence, ALPE offers a non-invasive approach to estimate key gas exchange variables—shunt fraction, dead space, and PaO_2/FiO_2 ratio—using only incremental FiO_2 adjustments, avoiding the need for more invasive devices such as arterial or central venous lines. Despite its innovation, ALPE has not gained widespread ICU adoption. Its technical complexity requires careful synchronization of ventilator settings, gas analysis, and software, along with multiple FiO_2 steps, which can be challenging in critically ill patients. The procedure is time-consuming, requires hemodynamic stability, and its interpretation demands specialized expertise. Moreover, simpler and faster methods to assess shunt, dead space, and the PaO_2/FiO_2 ratio are already routinely used in clinical practice. ICU patients are typically intubated and mechanically ventilated, with both central venous and arterial lines in place for blood gas sampling. These settings allow direct measurement of $EtCO_2$, as well as arterial and venous oxygen content, enabling the calculation of the aforementioned gas exchange variables without the need for additional equipment. Despite the relevant physiological insights that ALPE provides, the

cost and maintenance of the dedicated equipment further limit its daily clinical application in ICU.

Section 2—Lung imaging in detecting pulmonary dead space

As previously discussed, pulmonary dead space is traditionally estimated through volumetric capnography or physiological formulas such as the Bohr-Enghoff equation. However, these approaches provide only indirect and global measurements, making regional assessment challenging. Recent advances in lung imaging have opened new avenues for evaluating dead space distribution by combining anatomical and functional insights. Imaging techniques such as contrast-enhanced computed tomography (CT), dual-energy CT (DECT), magnetic resonance imaging (MRI), and increasingly, electrical impedance tomography (EIT) offer novel opportunities to visualize and quantify regional ventilation-perfusion (V/Q) mismatch, particularly in detecting ventilated but non-perfused areas representing alveolar dead space [43, 44]

Computed tomography and dual-energy techniques

Standard contrast-enhanced CT allows for high-resolution anatomical visualization of pulmonary structures and has been widely employed to detect embolic phenomena or vascular pruning—two important contributors to increased dead space. However, conventional CT offers limited functional insight into V/Q matching. In contrast to conventional CT, DECT provides not only anatomical but also functional information. It can distinguish between lung regions that are well perfused with iodine-based contrast and those that are not, allowing for detailed regional perfusion mapping. When combined with inhaled gas as contrast agent—such as Xenon [45]. DECT can also provide ventilation maps. By integrating both perfusion and ventilation data, DECT enables a direct evaluation of V/Q mismatch [46, 47]. Despite its strengths, DECT remains constrained by radiation exposure, cost, and the need for contrast agents, limiting its application for serial monitoring in the intensive care setting.

Magnetic resonance imaging

Pulmonary MRI, especially using hyperpolarized gases such as helium-3 or xenon-129, offers a radiation-free method for assessing regional ventilation. When combined with arterial spin labeling or contrast-based perfusion sequences, MRI can also capture pulmonary perfusion. MRI thus holds promise for non-invasive, detailed mapping of V/Q distribution [48]. However, technical limitations, availability, and logistical complexity—particularly in critically ill or ventilated patients—present barriers to routine use in the Intensive Care Unit (ICU).

Electrical impedance tomography: toward real-time, bedside V/Q assessment

EIT represents a transformative technology in this landscape. This bedside, radiation-free, real-time imaging tool uses surface electrodes to generate cross-sectional maps of lung impedance changes, closely reflecting ventilation dynamics in different settings [49, 50]. While conventionally used to monitor regional ventilation, recent developments in EIT have extended its reach into the assessment of pulmonary perfusion [51]. One way for assessing pulmonary perfusion with EIT is the bolus technique. In this approach, a contrast agent—typically hypertonic saline—is rapidly injected through a central venous line during a brief breath-hold. As the bolus travels through the right heart and pulmonary vasculature, it produces a transient decrease in electrical impedance within perfused lung regions. EIT captures these changes and, through dedicated algorithms, reconstructs a regional perfusion map. Although this technique does not provide absolute quantitative perfusion values, it offers a bedside, radiation-free, and repeatable method to assess regional pulmonary perfusion, particularly valuable in ICU setting [51, 52]. Pulmonary perfusion assessed using EIT has been compared with several imaging modalities, showing promising results [53, 54]. Studies have demonstrated that EIT-derived perfusion maps closely correspond with those obtained from CT [55, 56] and single-photon emission computed tomography (SPECT) [51]. Additionally, comparisons between EIT and positron emission tomography (PET) perfusion measurements have also shown encouraging findings, supporting the accuracy and reliability of EIT in evaluating regional lung perfusion [57]. These results highlight the potential of EIT as a non-invasive, bedside tool for real-time monitoring of pulmonary perfusion, especially in situations where conventional imaging methods are impractical or unavailable. When combined with simultaneous ventilation data, EIT enables bedside mapping of V/Q distribution. The ability to identify ventilated but not perfused regions—indicative of dead space—makes EIT a valuable tool for dynamic monitoring of lung function. This is particularly relevant in conditions such as ARDS, pulmonary embolism, or during extracorporeal support, where V/Q mismatch plays a central role in disease progression and management. Importantly, EIT offers the potential to guide real-time adjustments to ventilatory and hemodynamic strategies, helping to optimize oxygen delivery and reduce the risk of ventilator-induced lung injury (VILI). In a recent case report from our group, we highlighted how EIT perfusion imaging anticipated the clinical

diagnosis of pulmonary embolism and supported a more personalized approach to positive end-expiratory pressure (PEEP) titration, aimed at improving V/Q matching [58].

Despite its promising potential, EIT presents several technical and methodological limitations. First, current devices generate two-dimensional cross-sectional images, which may not fully capture the complex three-dimensional structure of the lungs. Although three-dimensional reconstruction approaches have been proposed, these remain confined to research settings and are not routinely used in clinical practice [52]. Furthermore, image quality and accuracy depend on correct belt positioning and optimal electrode-skin contact, both of which can be affected by patient habitus, body movement, or the presence of dressings and devices. Finally, quantitative perfusion imaging with EIT provides relative rather than absolute perfusion estimates and lacks full methodological standardization [59]. In conclusions, while traditional imaging modalities such as CT and MRI have enriched our understanding of pulmonary perfusion and ventilation, their use for assessing dead space in clinical practice remains limited by logistical and technical constraints. In contrast, EIT is performed entirely at the bedside, free of radiation, and can be repeated frequently without patient transport. These characteristics make it a practical tool for serial assessment of ventilation-perfusion distribution even in unstable patients [58, 60]. Its integration into critical care practice may further advance bedside monitoring of lung function, supporting more personalized respiratory management in critically ill patients.

Section 3—applications

In the following section, we present several illustrative cases to highlight the significance of dead space assessment in the management and monitoring of respiratory failure. These cases underscore how evaluating dead space can guide therapeutic decisions and improve patient outcomes.

Case 1: ARDS—assessment of lung recruitment and prone positioning response

The clinical case presented is entirely fictitious and was developed exclusively for educational purposes. A 36-year-old male with no prior medical history was admitted to the ICU for ARDS caused by H1N1 influenza. The patient, under deep sedation and paralysis, was placed on protective mechanical ventilation using the volume-controlled mode. There were no signs of hemodynamic, renal, hepatic, or coagulative dysfunction.

Below are the relevant ventilatory and arterial blood gas analysis (BGA) parameters:

Ventilatory parameters				Arterial BGA			
VT	480	Pplat	22	pH	7.35	P_aO2/F_iO2	146
RR	24	DP	10	$PaCO_2$	48	Shunt	0.27
Ve	11.52	CRS	48	PO_2	95		
PEEP	12	$EtCO_2$	24	FiO_2	0.65		

On day 1, the patient underwent a recruitment maneuver, which consisted of applying a sustained inflation with positive pressure of 40 cmH_2O for 20 s. There were no signs of hemodynamic instability, after which PEEP was increased from 12 to 14 cmH_2O.

Following the maneuver, the following changes were observed:

- PO_2 increased to 105 mmHg
- $PaO2/FiO_2$ ratio improved to 161
- Respiratory system compliance (CRS) improved from 48 to 53
- $PaCO_2$ and $EtCO_2$ remained unchanged

Can we consider the patient responsive to the recruitment maneuver?

At present, there are no clear or universally accepted criteria to reliably determine a patient's response to a recruitment maneuver [61], and current scientific evidence does not support an aggressive approach involving recruitment maneuvers or high PEEP levels in the management of ARDS [62]. However, a significant reduction in alveolar dead space—rather than an increase in the PaO_2/FiO_2 ratio or improvements in respiratory mechanics—may be a more reliable indicator of a positive response to recruitment.

Before the maneuver, the alveolar dead space was calculated as

Alveolar Dead Space = (48 − 24)/48 = 0.5

Considering the modest increase in PaO_2/FiO_2 and CRS, and the fact that $PaCO_2$, $EtCO_2$, and consequently the dead space did not change, the response to the recruitment maneuver appears to be minimal or even absent.

The patient then underwent a 16-h pronation cycle. After pronation, the PaO_2/FiO_2, shunt, and CRS remained unchanged, while $PaCO_2$ increased to 56 mmHg. This elevated $PaCO_2$ could be mistakenly interpreted as a negative response to the pronation maneuver, especially without considering the $EtCO_2$, which rose to 32 mmHg.

The alveolar dead space after the pronation cycle was calculated as:

Alveolar Dead Space = (56 − 32)/56 = 0.42

Upon reassessing the alveolar dead space, a reduction from 0.5 to 0.42 was noted. This reduction indicates that

the lung reopening was effective, as reflected by the clear improvement in alveolar ventilation.

Take-home messages:

– When assessing lung reopening through pronation, recruitment maneuvers, or PEEP titration, always evaluate the dead space fraction before and after the intervention [63, 64].

Case 2: ARDS and dead space overestimation

The clinical case presented is entirely fictitious and was developed exclusively for educational purposes. A 45-year-old female with no prior health issues was admitted to the ICU for severe ARDS caused by a pneumococcal infection.

The patient, under deep sedation and paralysis, was placed on protective mechanical ventilation using the volume-controlled mode. There were no signs of hemodynamic, renal, hepatic, or coagulative dysfunction.

Here are the relevant ventilatory and arterial blood gas analysis (BGA) parameters:

Ventilatory parameters				Arterial BGA			
VT	380	Pplat	24	pH	7.29	P_aO2/F_iO_2	95
RR	28	DP	10	$PaCO_2$	57	Shunt	0.42
Ve	10.64	CRS	38	PO_2	95		
PEEP	14	$EtCO_2$	25	FiO_2	100		

At the patient's presentation, the alveolar dead space was calculated as:

Alveolar Dead Space = (57 − 25)/57 = 0.56

In this case, the alveolar dead space value is significantly influenced by the high level of venous admixture. The Enghoff modification of the dead space formula replaces the mean $PACO_2$ with the $PaCO_2$. As the shunt fraction increases—especially when it exceeds 0.4—$PaCO_2$ rises substantially, while $PACO_2$ decreases. This discrepancy results in a consistent overestimation of dead space. However, despite this overestimation in absolute terms, alveolar dead space over time remains a valuable and reliable marker of disease severity.

Take-home messages:

– When calculating dead space, the level of pulmonary shunt should always be considered. A shunt fraction greater than 0.4 can cause significant dead space overestimation [65].
– With a high-constant level of pulmonary shunt, the trend in dead space values remains reliable [66].

Case 3: severe asthma and dead space interpretation

The clinical case presented is entirely fictitious and was developed exclusively for educational purposes. A 25-year-old male with no significant past medical history was admitted to the ICU for management of severe asthma.

The patient, under deep sedation and paralysis, was placed on mechanical ventilation using the volume-controlled mode. No signs of hemodynamic, renal, hepatic, or coagulative dysfunction were present.

Here are the relevant ventilatory and arterial blood gas analysis (BGA) parameters:

Ventilatory parameters				Arterial BGA			
VT	650	Ppeak	53	pH	7.29	P_aO2/F_iO_2	271
RR	8	Pplat	24	$PaCO_2$	57	Shunt	0.11
Ve	5.2	DP	10	PO_2	95		
PEEP	0	CRS	65	FiO_2	0.35		
PEEPi	14	$EtCO_2$	63				

At the patient's presentation, the alveolar dead space was calculated as follows:

Alveolar Dead Space = (57 − 63)/57 = − 0.10

Can Dead Space Be Negative?

Paradoxically, in certain pathological conditions, the $EtCO_2$ can be higher than $PaCO_2$. This phenomenon is particularly observed in severe obstructive respiratory diseases like asthma. During such conditions, CO_2 transferred from the capillary blood to the alveoli can become trapped due to airway obstruction. Alveoli that fail to expel CO_2 because of this obstruction act as a reservoir for the gas. When this "stored" CO_2 is eventually exhaled, the CO_2 measured at the end of the airway ($EtCO_2$) does not truly reflect the $PaCO_2$ but rather the CO_2 that had been retained in the alveoli.

In cases of severe airway obstruction, the dead space computation can be highly unreliable. Therefore, before calculating dead space, it is essential to first assess the steady state of CO_2 production and elimination, which can be confirmed by a constant $PaCO_2$ value and a plateau in $EtCO_2$.

Take-home messages:

– Dead space computation during severe obstructive pulmonary diseases, such as asthma, can be unreliable [67].
– Dead space computation should always be preceded by the assessment of the CO_2 production-elimination steady state [68].

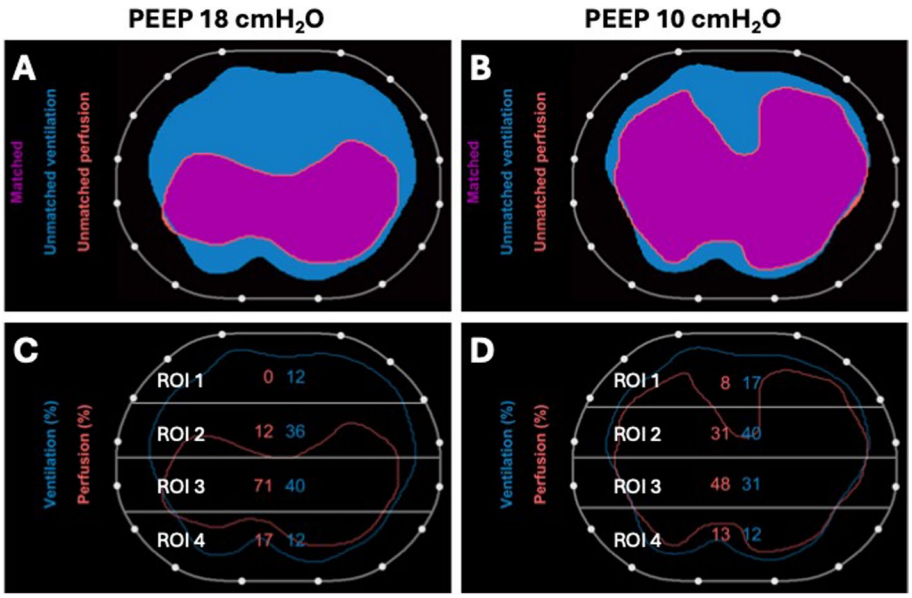

Fig. 5 EIT perfusion study of the patient at PEEP 18 cmH_2O and PEEP 10 cmH_2O. **A** shows the areas of unmatched ventilation, unmatched perfusion, and matched ventilation-perfusion regions at PEEP 18 cmH_2O. **B** displays the corresponding areas at PEEP 10 cmH_2O. Reducing PEEP from 18 to 10 cmH_2O resulted in a marked decrease in unmatched ventilation, from 55.2 to 20.7%, and a corresponding increase in matched regions, from 44.5 to 79.1%. **C** illustrates the percentage distribution of perfusion (red) and ventilation (blue) across four horizontal regions of interest (ROIs), where ROIs 1 and 2 represent the non-dependent lung regions and ROIs 3 and 4 correspond to the dependent regions. At PEEP 15 cmH_2O, perfusion was predominantly confined to the dependent regions (88%) compared to the non-dependent regions (12%), while ventilation was evenly distributed (48% non-dependent, 52% dependent). **D** shows that after reducing PEEP to 10 cmH_2O, perfusion became more evenly distributed, with 39% in the non-dependent regions and 61% in the dependent regions. Ventilation showed a slight shift toward the non-dependent regions, with 57% in the non-dependent areas and 43% in the dependent areas

Case 4: regional dead space estimation using EIT

A 70-year-old man with intellectual disability secondary to chronic brain disease, otherwise healthy, was diagnosed with viral pneumonia due to COVID-19. Informed consent was obtained for the publication of his anonymized case.

Due to refractory respiratory failure unresponsive to maximal non-invasive therapy, the patient was intubated and placed on protective mechanical ventilation using pressure-regulated volume control (PRVC). Once stabilized, an EIT study was conducted to assess regional ventilation and perfusion. For the perfusion evaluation, a bolus of 10 mL of 5% hypertonic saline was injected through a central venous catheter placed in the jugular vein during an inspiratory breath hold.

Here are the relevant ventilatory and BGA parameters:

Ventilatory parameters				**Arterial BGA**			
VT	480	Pplat	30	pH	7.38	P_aO2/F_iO_2	245
RR	18	DP	12	$PaCO_2$	46	Shunt	0.15
Ve	8.6	Crs	40	PO_2	135		
PEEP	18	$EtCO_2$	33	FiO_2	0.55		
PEEPi	0						

The EIT study revealed a ventilation-perfusion match of 44.5% with a percentage of unmatched ventilation (i.e., dead space) of 55.2%. Perfusion was predominantly distributed in the dependent lung regions (88%), while it was markedly reduced in the non-dependent regions (12%). Ventilation was evenly distributed, with 48% in the non-dependent regions and 52% in the dependent regions. Unmatched perfusion was negligible (0.4%).

At this point, a decremental PEEP trial was performed to optimize ventilatory settings. The optimal PEEP level was identified as 10 cmH_2O.

The parameters changed as follows:

Ventilatory parameters				**Arterial BGA**			
VT	480	Pplat	18	pH	7,41	P_aO2/F_iO_2	164
RR	18	DP	7	$PaCO_2$	43	Shunt	0.18
Ve	8.6	Crs	69	PO_2	90		
PEEP	10	$EtCO_2$	31	FiO_2	0.55		
PEEPi	1						

A repeat EIT study showed an improvement in ventilation-perfusion matching, which increased to 79.1%, while the proportion of unmatched ventilation (dead space) decreased to 20.7%. Perfusion also became more evenly

distributed, with 39% in the non-dependent regions and 61% in the dependent regions. Ventilation showed a slight shift toward the non-dependent regions, with 57% in the non-dependent areas and 43% in the dependent areas. Unmatched perfusion was 0.2% (Fig. 5).

Take-home messages:

- EIT, combined with hypertonic saline injection, allows for non-invasive, regional assessment of areas of unmatched ventilation, unmatched perfusion and ventilation/perfusion matching.
- EIT enables the assessment of perfusion changes and ventilation-perfusion matching following interventions such as PEEP adjustments, making it a valuable tool to support the clinical management of critically ill patients.

Limitations

Dead space is a key parameter for assessing respiratory failure severity, reflecting the proportion of ventilation not involved in gas exchange. Its calculation assumes that $PACO_2$ equals $PaCO_2$—an approximation that may be inaccurate in cases of massive pulmonary shunt, potentially leading to misestimation of the dead space fraction. Dead space alone does not provide information on the global or regional distribution of ventilation–perfusion (V/Q) mismatch. Identifying the spatial pattern of V/Q abnormalities requires advanced and costly tools such as electrical impedance tomography (EIT), positron emission tomography (PET), or dual-energy computed tomography (DECT), along with high operator expertise—resources not always available in routine practice.

Future directions

Dead space estimation remains a clinically relevant parameter, capable of providing valuable insights into the severity and progression of lung injury in critically ill patients with respiratory failure. Its role at the bedside is likely to expand in the coming years, supported by technological advances and a growing understanding of ventilation–perfusion (V/Q) pathophysiology. Potential areas for future research and clinical application include:

- Integration of dead space quantification with V/Q distribution mapping in daily practice. Combining volumetric capnography derived dead space measurements with advanced imaging modalities such as EIT, DECT, or PET could allow a more comprehensive, real-time evaluation of both the magnitude and spatial distribution of V/Q mismatch.
- Longitudinal analysis of dead space trends. Monitoring changes in dead space over the course of illness or treatment may help characterize disease trajectories, identify early signs of deterioration, and assess response to interventions.
- Ventilatory strategies guided by dead space and V/Q imaging. Tailoring ventilator settings based on dead space values and regional V/Q data could optimize gas exchange while minimizing ventilator-induced lung injury, potentially improving outcomes in patients with heterogeneous lung disease.
- Integration of Artificial Intelligence (AI). AI may help integrate heterogeneous sources of information, such as ventilator waveforms, capnography and imaging data from EIT to provide a more complete assessment of V/Q matching including changes in dead space. Such integration could help optimize and personalize ventilation strategies at the bedside.

Conclusion

Dead space is a key physiological variable that provides crucial insights into the pathophysiology of respiratory failure. Understanding the mathematical foundations of dead space calculation, as well as the interpretation of its key components—such as $EtCO_2$, $PaCO_2$, and $PECO_2$—is essential for accurate assessment and clinical application. Complementary indices, including the ventilatory ratio and standardized minute ventilation, can further support the evaluation of respiratory failure severity. Today, dead space is no longer merely a mathematical construct. Advances in technology, such as electrical impedance tomography, now allow it to be visualized and mapped, offering new perspectives on regional ventilation–perfusion relationships.

We believe that mastering these concepts can significantly enhance the clinician's ability to interpret and apply dead space measurements in daily practice.

Abbreviations

ARDS	Acute respiratory distress syndrome
BGA	Blood gas analysis
BW	Body weight
CO_2	Carbon dioxide
CRS	Respiratory system Compliance
CT	Computed tomography
DECT	Dual-energy CT
DP	Driving pressure
EIT	Electrical impedance tomography
$EtCO_2$	End-tidal CO_2
FCO_2	Fraction of CO_2
ICU	Intensive care unit
MRI	Magnetic resonance imaging
$PACO_2$	Alveolar partial pressure CO_2
$PaCO_2$	Arterial partial pressure of CO_2
Patm	Atmospheric pressure

$PECO_2$	Mixed expiratory CO_2
PEEP	Positive and expiratory pressure
PEEPi	Intrinsic positive and expiratory pressure
PET	Positron emission tomography
Ppeak	Airway peak pressure
Pplat	Plateau pressure
PRVC	Pressure-regulated volume control
Pvap	Water vapor pressure
RR	Respiratory rate
SPECT	Single-photon emission computed tomography
SV	Standardized minute ventilation
VA	Alveolar ventilation
VCO_2	Volume of CO_2 per minute
VD	Dead space
VD/VT	Dead space fraction
Ve	Minute ventilation
VILI	Ventilator-induced lung injury
V/Q	Ventilation–perfusion mismatch
VR	Ventilatory ratio
VT	Tidal volume

Acknowledgements
Not applicable.

Authors' contributions
FC conceived the study, searched literature and wrote the manuscript. AS revised the manuscript. RG searched literature, wrote the manuscript and provided figures. SL revised the manuscript. MF provided figures and revised the manuscript. GB and GF revised the manuscript. ER conceived the study, searched literature, wrote the manuscript, provided figures and supervised the study project.

Funding
This study was supported by Institutional funds at the University of Milano-Bicocca, Monza, Italy.

Data availability
Data are available upon reasonable request to the corresponding author.

Declarations

Consent for publication
The patient of case 4 provided informed consent for the publication of the anonymized case.

Competing interests
The authors declare no competing interests.

Received: 13 October 2025 Accepted: 18 November 2025
Published online: 09 January 2026

References

1. Lagina M, Valley TS (2024) Diagnosis and management of acute respiratory failure. Crit Care Clin 40:235–253
2. Rezoagli E, Fumagalli R, Bellani G (2017) Definition and epidemiology of acute respiratory distress syndrome. Ann Transl Med 5(14):282
3. Lellouche F, Delorme M, Brochard L (2020) Impact of respiratory rate and dead space in the current era of lung protective mechanical ventilation. Chest 158:45–47
4. Raimondi Cominesi D, Forcione M, Pozzi M, Giani M, Foti G, Rezoagli E, Cipulli F (2024) Pulmonary shunt in critical care: a practical approach with clinical scenarios. J Anesth Analg Crit Care 4(1):18
5. Bhalla AK, Chau A, Khemani RG, Newth CJL (2023) The end-tidal alveolar dead space fraction for risk stratification during the first week of invasive mechanical ventilation: an observational cohort study. Crit Care 27:54
6. Nuckton TJ, Alonso JA, Kallet RH, Daniel BM, Pittet J-F, Eisner MD, Matthay MA (2002) Pulmonary dead-space fraction as a risk factor for death in the acute respiratory distress syndrome. N Engl J Med 346:1281–1286
7. Rezoagli E, Laffey JG, Bellani G (2022) Monitoring lung injury severity and ventilation intensity during mechanical ventilation. Semin Respir Crit Care Med 43:346–368
8. Raurich JM, Vilar M, Colomar A, Ibáñez J, Ayestarán I, Pérez-Bárcena J, Llompart-Pou JA (2010) Prognostic value of the pulmonary dead-space fraction during the early and intermediate phases of acute respiratory distress syndrome. Respir Care 55:282–287
9. Intagliata S, Rizzo A, Gossman W (2024) Physiology, Lung Dead Space StatPearls (Treasure Island (FL): StatPearls Publishing)
10. Willner D, Weissman C (2011) Carbon dioxide production, metabolism, and anesthesia Capnography ed J S Gravenstein, M B Jaffe, N Gravenstein and D A Paulus (Cambridge University Press) pp 239–49
11. Doyle J, Cooper JS (2024) Physiology, carbon dioxide transport. StatPearls (Treasure Island (FL): StatPearls Publishing)
12. Singer P (2016) Simple equations for complex physiology: can we use VCO2 for calculating energy expenditure? Crit Care 20:72
13. Robertson HT (2015) Dead space: the physiology of wasted ventilation. Eur Respir J 45:1704–1716
14. Bohr C (1891) Ueber die Lungenathmung[1] Skandinavisches Archiv Für Physiologie 2:236–68
15. West JB (2019) Three classical papers in respiratory physiology by Christian Bohr (1855–1911) whose work is frequently cited but seldom read. Am J Physiol-Lung Cell Molecul Physiol 316:L585-8
16. Benner A, Lewallen N F and Sharma S (2024) Physiology, Carbon Dioxide Response Curve StatPearls (Treasure Island (FL): StatPearls Publishing)
17. West JB (1977) State of the art: ventilation-perfusion relationships. Am Rev Respir Dis 116(5):919–943
18. Nunn JF, Holmdahl MH (1979) Henrik Enghoff and the Volumen Inefficax. Ups J Med Sci 84:105–108
19. Severinghaus JW (2002) The invention and development of blood gas analysis apparatus. Anesthesiology 97:253–256
20. Severinghaus JW, Astrup PB (1985) History of blood gas analysis. I. The development of electrochemistry. J Clin Monit Comput 1(3):180–192
21. Maj R, Palermo P, Gattarello S, Brusatori S, D'Albo R, Zinnato C, Velati M, Romitti F, Busana M, Wieditz J, Herrmann P, Moerer O, Quintel M, Meissner K, Sanderson B, Chiumello D, Marini JJ, Camporota L, Gattinoni L (2023) Ventilatory ratio, dead space, and venous admixture in patients with acute respiratory distress syndrome. Br J Anaesth 130:360–7
22. Doorduin J, Nollet JL, Vugts MPAJ, Roesthuis LH, Akankan F, van der Hoeven JG, van Hees HWH, Heunks LMA (2016) Assessment of dead-space ventilation in patients with acute respiratory distress syndrome: a prospective observational study. Crit Care 20:121
23. Sayah AJ, Peacock WF, Overton DT (1990) End-tidal CO2 measurement in the detection of esophageal intubation during cardiac arrest. Ann Emerg Med 19:857–60
24. Owens B, Hall C (2024) Application of end-tidal CO2 monitoring to ICU management. Crit Care Nurs Q 47:157–62
25. Zwerneman K (2006) End-tidal carbon dioxide monitoring: a VITAL sign worth watching. Crit Care Nurs Clin North Am 18:217–25
26. Beitler JR, Thompson BT, Matthay MA, Talmor D, Liu KD, Zhuo H, Hayden D, Spragg RG, Malhotra A (2015) Estimating dead-space fraction for secondary analyses of acute respiratory distress syndrome clinical trials. Crit Care Med 43:1026–1035
27. Verscheure S, Massion PB, Verschuren F, Damas P, Magder S (2016) Volumetric capnography: lessons from the past and current clinical applications. Crit Care 20:184
28. Kreit JW (2019) Volume capnography in the intensive care unit: physiological principles, measurements, and calculations. Annals ATS AnnalsATS.201807-501CME
29. Hastings RH, Powell FL (1986) Physiological dead space and effective parabronchial ventilation in ducks. J Appl Physiol 60:85–91
30. Zheng M (2023) Dead space ventilation-related indices: bedside tools to evaluate the ventilation and perfusion relationship in patients with acute respiratory distress syndrome. Crit Care 27:46
31. Rezoagli E, Laffey J G, Madotto F, Protti A, Pham T, Pesenti A, Bellani G, Brochard L (2025) Prognostic value of disease severity and mechanical ventilation intensity in Acute Respiratory Distress Syndrome. Analysis of the LUNG SAFE cohort. Eur Respir J 2500742

32. Sinha P, Sanders RD, Soni N, Vukoja MK, Gajic O (2013) Acute Respiratory Distress Syndrome: The Prognostic Value of Ventilatory Ratio—A Simple Bedside Tool to Monitor Ventilatory Efficiency. Am J Respir Crit Care Med 187:1150–3
33. Sinha P, Calfee CS, Beitler JR, Soni N, Ho K, Matthay MA, Kallet RH (2019) Physiologic analysis and clinical performance of the ventilatory ratio in acute respiratory distress syndrome. Am J Respir Crit Care Med 199:333–341
34. Torres A, Motos A, Riera J, Fernández-Barat L, Ceccato A, Pérez-Arnal R, García-Gasulla D, Peñuelas O, Lorente JA, Rodriguez A, De Gonzalo-Calvo D, Almansa R, Gabarrús A, Menéndez R, Bermejo-Martin JF, Ferrer R, Amaya Villar R, Añón JM, Barberà C, Barberán J, Blandino Ortiz A, Bustamante-Munguira E, Caballero J, Carbajales C, Carbonell N, Catalán-González M, Galbán C, Gumucio-Sanguino VD, De La Torre MDC, Díaz E, Estella Á, Gallego E, García Garmendia JL, Garnacho-Montero J, Gómez JM, Huerta A, Jorge García RN, Loza-Vázquez A, Marin-Corral J, Martínez De La Gándara A, Martínez Varela I, López Messa J, Albaiceta GM, Novo M A, Peñasco Y, Pozo-Laderas JC, Ricart P, Salvador-Adell I, Sánchez-Miralles A, Sancho Chinesta S, Socias L, Solé-Violan J, Suares Sipmann F, Tamayo Lomas L, Trenado J, Barbé F, CIBERESUCICOVID Project (COV20/00110, ISCIII), Adell-Serrano B, Agrifoglio A, Aguilar Cabello M, Aguilera L, Alcaraz-Serrano V, Aldecoa C, Alegre C, Álvarez S, Álvarez Ruiz A, Andrea R, Ángel J, Arrieta M, Ayestarán JI, Badia J R, Badía M, Báez Pravia O, Mariño A B, Balsera B, Barbena L, Barbeta E, Bardi T, Barral Segade P, Barroso M, Berezo García JÁ, Bigas J, Blancas R, Blasco Cortés ML, Boado M, Bodi Saera M, Bofill N, Bouza Vieiro MT, Bueno L, Bustamante-Munguira J, Cachafeiro L, Campi Hermoso D, Campos Fernández S, Cano I, Cantón-Bulnes ML, Cardina Fernández P, Carrión García L, Carvalho S, et al (2021) The evolution of the ventilatory ratio is a prognostic factor in mechanically ventilated COVID-19 ARDS patients. Crit Care 25:331
35. Fischbach A, Wiegand SB, Simons JA, Ammon L, Kopp R, Soccoro Matos GI, Baigorri JJ, Crowley JC, Bagchi A (2024) The ventilatory ratio as a predictor of successful weaning from a veno-venous extracorporeal membrane oxygenator. JCM 13(13):3758
36. Parada-Gereda HM, Avendaño JM, Melo JE, Ruiz CI, Castañeda MI, Medina-Parra J, Merchán-Chaverra R, Corzzo D, Molano-Franco D, Masclans JR (2023) Association between ventilatory ratio and mortality in patients with acute respiratory distress syndrome and COVID 19: a multicenter, retrospective cohort study. BMC Pulm Med 23:425
37. Forster HV, Pan LG, Bisgard GE, Flynn C, Hoffer RE (1986) Effect of reducing anatomic dead space on arterial PCO2 during CO2 inhalation. J Appl Physiol 61:728–733
38. Yamanaka MK, Sue DY (1987) Comparison of arterial-end-tidal PCO2 difference and dead space/tidal volume ratio in respiratory failure. Chest 92:832–835
39. Bonifazi M, Romitti F, Busana M, Palumbo MM, Steinberg I, Gattarello S, Palermo P, Saager L, Meissner K, Quintel M, Chiumello D, Gattinoni L (2021) End-tidal to arterial PCO2 ratio: a bedside meter of the overall gas exchanger performance. Intensive Care Med Exp 9:21
40. Waldau T, Larsen VH, Parbst H, Bonde J (2002) Assessment of the respiratory exchange ratio in mechanically ventilated patients by a standard anaesthetic gas analyser. Acta Anaesthesiol Scand 46:1242–1250
41. Rees SE, Kjærgaard S, Thorgaard P, Malczynski J, Toft E, Andreassen S (2002) The automatic lung parameter estimator (ALPE) system: non-invasive estimation of pulmonary gas exchange parameters in 10-15 minutes. J Clin Monit Comput 17:43–52
42. Riley RL, Cournand A (1949) Ideal alveolar air and the analysis of ventilation-perfusion relationships in the lungs. J Appl Physiol 1:825–847
43. Gaulton TG, Xin Y, Victor M, Nova A, Cereda M (2024) Imaging the pulmonary vasculature in acute respiratory distress syndrome. Nitric Oxide 147:6–12
44. Cereda M, Xin Y, Goffi A, Herrmann J, Kaczka DW, Kavanagh BP, Perchiazzi G, Yoshida T, Rizi RR (2019) Imaging the injured lung: mechanisms of action and clinical use. Anesthesiology 131:716–749
45. Herrmann J, Gerard SE, Reinhardt JM, Hoffman EA, Kaczka DW (2021) Regional gas transport during conventional and oscillatory ventilation assessed by xenon-enhanced computed tomography. Ann Biomed Eng 49:2377–2388
46. Vlahos I, Jacobsen MC, Godoy MC, Stefanidis K, Layman RR (2022) Dual-energy CT in pulmonary vascular disease. Br J Radiol 95:20210699
47. Hong YJ, Shim J, Lee SM, Im DJ, Hur J (2021) Dual-energy CT for pulmonary embolism: current and evolving clinical applications. Korean J Radiol 22:1555
48. Wielpütz M, Kauczor HU. MRI of the lung: state of the art. Diagn Interv Radiol. 2012;18(4):344–53. https://doi.org/10.4261/1305-3825.DIR.5365-11.0. Epub 2012 Mar 20. PMID: 22434450.
49. Bronco A, Grassi A, Meroni V, Giovannoni C, Rabboni F, Rezoagli E, Teggia-Droghi M, Foti G, Bellani G (2021) Clinical value of electrical impedance tomography (EIT) in the management of patients with acute respiratory failure: a single centre experience. Physiol Meas 42(7):074003
50. Bastia L, Garberi R, Querci L, Cipolla C, Curto F, Rezoagli E, Fumagalli R, Chieregato A (2024) Dynamic inflation prevents and standardized lung recruitment reverts volume loss associated with percutaneous tracheostomy during volume control ventilation: results from a Neuro-ICU population. J Clin Monit Comput 38:1387–1396
51. Borges JB, Suarez-Sipmann F, Bohm SH, Tusman G, Melo A, Maripuu E, Sandström M, Park M, Costa ELV, Hedenstierna G, Amato M (2012) Regional lung perfusion estimated by electrical impedance tomography in a piglet model of lung collapse. J Appl Physiol 112:225–236
52. Scaramuzzo G, Pavlovsky B, Adler A, Baccinelli W, Bodor DL, Damiani LF, Franchineau G, Francovich J, Frerichs I, Giralt JAS, Grychtol B, He H, Katira BH, Koopman AA, Leonhardt S, Menga LS, Mousa A, Pellegrini M, Piraino T, Priani P, Somhorst P, Spinelli E, Händel C, Suárez-Sipmann F, Wisse JJ, Becher T, Jonkman AH (2024) Electrical impedance tomography monitoring in adult ICU patients: state-of-the-art, recommendations for standardized acquisition, processing, and clinical use, and future directions. Crit Care 28:377
53. Putensen C, Hentze B, Muenster S, Muders T (2019) Electrical impedance tomography for cardio-pulmonary monitoring. JCM 8(8):1176
54. Spinelli E, Kircher M, Stender B, Ottaviani I, Basile MC, Marongiu I, Colussi G, Grasselli G, Pesenti A, Mauri T (2021) Unmatched ventilation and perfusion measured by electrical impedance tomography predicts the outcome of ARDS. Crit Care 25:192
55. Frerichs I, Hinz J, Herrmann P, Weisser G, Hahn G, Quintel M, Hellige G (2002) Regional lung perfusion as determined by electrical impedance tomography in comparison with electron beam CT imaging. IEEE Trans Med Imaging 21(6):646–652
56. Martin KT, Xin Y, Gaulton TG, Victor M, Santiago RR, Kim T, Morais CCA, Kazimi AA, Connell M, Gerard SE, Herrmann J, Mueller AL, Lenart A, Shen J, Khan SS, Petrov M, Reutlinger K, Rozenberg K, Amato M, Berra L, Cereda M (2023) Electrical impedance tomography identifies evolution of regional perfusion in a porcine model of acute respiratory distress syndrome. Anesthesiology 139:815–826
57. Bluth T, Kiss T, Kircher M, Braune A, Bozsak C, Huhle R, Scharffenberg M, Herzog M, Roegner J, Herzog P, Vivona L, Millone M, Dössel O, Andreeff M, Koch T, Kotzerke J, Stender B, Gama De Abreu M (2019) Measurement of relative lung perfusion with electrical impedance and positron emission tomography: an experimental comparative study in pigs. Br J Anaesth 123(2):246–254
58. Garberi R, Ripa C, Carenini G, Bastia L, Giani M, Foti G, Rezoagli E (2025) Personalized ventilation guided by electrical impedance tomography with increased PEEP improves ventilation-perfusion matching in asymmetrical airway closure and contralateral pulmonary embolism during veno-venous extracorporeal membrane oxygenation: a case report. Physiol Rep 13(7):e70280
59. Xu M, He H, Long Y (2021) Lung perfusion assessment by bedside electrical impedance tomography in critically ill patients. Front Physiol 12:748724
60. Bronco A, Fazzi F, Amendolagine L, Garberi R, Cattaneo S, Ferrari F, Bonanomi E, Foti G, Rezoagli E (2025) Electrical impedance tomography in congenital heart disease: advancing non-invasive pulmonary perfusion assessment at bedside. ICMx 13(1):75
61. Rezoagli E, Bellani G (2019) How I set up positive end-expiratory pressure: evidence- and physiology-based! Crit Care 23(412):s13054-019-2695-z
62. Writing Group for the Alveolar Recruitment for Acute Respiratory Distress Syndrome Trial (ART) Investigators, Cavalcanti AB, Suzumura ÉA, Laranjeira LN, Paisani DDM, Damiani LP, Guimarães HP, Romano ER, Regenga MDM, Taniguchi LNT, Teixeira C, Pinheiro De Oliveira R, Machado FR, Diaz-Quijano FA, Filho MSDA, Maia IS, Caser EB, Filho WDO, Borges MDC, Martins PDA, Matsui M, Ospina-Tascón GA, Giancursi TS, Giraldo-Ramirez ND, Vieira SRR, Assef MDGPDL, Hasan MS, Szczeklik W, Rios F, Amato MBP, Berwanger O, Ribeiro De Carvalho CR (2017) Effect of lung recruitment

and titrated positive end-expiratory pressure (PEEP) vs low PEEP on mortality in patients with acute respiratory distress syndrome: a randomized clinical trial. JAMA 318:1335

63. De Rosa S, Sella N, Bellani G, Foti G, Cortegiani A, Lorenzoni G, Gregori D, Boscolo A, Cattin L, Elhadi M, Fullin G, Garofalo E, Gottin L, Grassetto A, Maggiore S M, Momesso E, Peta M, Poole D, Rona R, Tiberio I, Zanoletti A, Rezoagli E, Navalesi P, for the SIAARTI Study Group, Abastanotti M, Abdel-Maboud Abdel-Maboud M, Abdelmageed A A, Abdullah E, Abodina A M, Abuelyamen A, Abusalama A, Abuzaid T A, Aceto R, Addesa S, Alampi D, Aldhalia A, Alessio R, Al-juaifari M, Alqandouz R A, Al-Sadawi M, Anderloni M, Andrea C, Andriolo E, Anna B, Antonini B, Anzellotti G M, Aritzu M, Awad A K, Badii F, Bakeer H B, Bakri A, Ballin A, Barattini M, Barotti M, Bassi M, Bellandi M, Bellin M, Bellissima A, Benini A, Berruto F, Berta G, Berti M, Biagioni E, Biamonte E, Bianchetti G, Bianchin A, Biasetto M, Binnawara M, Bisi M, Bitondo M M, Boffa N, Bombino M, Bonazzi B, Bonetta E, Boni E, Borga S, Bosco V, Boscolo G, Bozzon V, Brazzi L, Bristot A, Brumana N, Bruni A, Bruscagnin C, Busani S, Bussone G, Caironi P, Calocero T, Campagnolo M, Canepa C, Carlon R, Carrara A, Castelli A, Catalisano G, Cavinato M, Ceccaroni F, Cecconi M, Cedrone M, et al (2025) Oxygenation improvement and duration of prone positioning are associated with ICU mortality in mechanically ventilated COVID-19 patients. Ann Intensive Care 15:20
64. Rezoagli E, Fornari C, Fumagalli R, Grasselli G, Volta CA, Navalesi P, Knafelj R, Brochard L, Pesenti A, Mauri T, Foti G, Pleural Pressure Working Group (PLUG), Colombo R, Cortegiani A, Zhou J-X, D'Andrea R, Calamai I, González ÁV, Roca O, Grieco DL, Jovaisa T, Bampalis D, Becher T, Battaglini D, Ge H, Luz M, Santos E, Constantin J-M, Ranieri M, Guerin C, Mancebo J, Pelosi P (2024) Heterogeneous impact of Sighs on mortality in patients with acute hypoxemic respiratory failure: insights from the PROTECTION study. Ann Intensive Care 14:153
65. Suarez-Sipmann F, Santos A, Böhm SH, Borges JB, Hedenstierna G, Tusman G (2013) Corrections of Enghoff's dead space formula for shunt effects still overestimate Bohr's dead space. Respir Physiol Neurobiol 189:99–105
66. Ong T, Stuart-Killion RB, Daniel BM, Presnell LB, Zhuo H, Matthay MA, Liu KD (2009) Higher pulmonary dead space may predict prolonged mechanical ventilation after cardiac surgery. Pediatr Pulmonol 44(5):457–463
67. Demoule A, Brochard L, Dres M, Heunks L, Jubran A, Laghi F, Mekontso-Dessap A, Nava S, Ouanes-Besbes L, Peñuelas O, Piquilloud L, Vassilakopoulos T, Mancebo J (2020) How to ventilate obstructive and asthmatic patients. Intensive Care Med 46:2436–2449
68. Siobal MS, Ong H, Valdes J, Tang J (2013) Calculation of physiologic dead space: comparison of ventilator volumetric capnography to measurements by metabolic analyzer and volumetric CO_2 monitor. Respir Care 58:1143–1151

Publisher's Note